Nonlinear Dyn (2021) 103:883–895
https://doi.org/10.1007/s11071-020-06040-4

ORIGINAL PAPER

Neural coupling mechanism in fMRI hemodynamics

Jun Peng · Yihong Wang · Rubin Wang · Wanzeng Kong · Jianhai Zhang

Received: 27 May 2020 / Accepted: 17 October 2020 / Published online: 6 January 2021

Abstract Neural activity alters with the changes in cerebral blood flow (CBF) and blood oxygen saturation. Despite that these changes can be detected with functional magnetic resonance imaging (fMRI), the underlying physiological mechanism remains obscure. Upon activation of the specific brain region, CBF increases substantially, albeit with 6–8 s delay. Neuroscience has no scientific explanation for this experimental discovery yet. This study proposed a physiological mechanism for generating hemodynamic phenomena from the perspective of energy metabolism. The ratio of reduction (NADH) and oxidation states (NAD^+) of nicotinamide adenine dinucleotide in cell was considered as the variable for CBF regulation. After the specific brain region was activated, brain glycogen was rapidly consumed as reserve energy, resulting in no significant change in the ratio of NADH and NAD^+ concentrations. However, when the stored energy in the cell is exhausted, the dynamic equilibrium state of the transition between NADH and NAD + is changed, and the ratio of NADH and NAD^+ concentrations is significantly increased, which regulates the blood flow to be greatly increased. Based on this physiological mechanism, this paper builds a large-scale visual nervous system network based on the Wang–Zhang neuron model, and quantitatively reproduced the hemodynamics observed in fMRI by computer numerical simulation. The results demonstrated that the negative energy mechanism, which was previously reported by our group using Wang–Zhang neuronal model, played a vital role in governing brain hemodynamics. Also, it precisely predicted the neural coupling mechanism between the energy metabolism and blood flow changes in the brain under stimulation. In nature, this mechanism is determined by imbalance and mismatch between the positive and negative energy during the spike of neuronal action potentials. A quantitative analysis was adopted to elucidate the physiological mechanism underlying this phenomenon, which would provide an insight into the principle of brain operation and the neural model of the overall brain function.

Keywords fMRI · Negative energy · Energetics coding · Hemodynamics · Neural network · Brain glycogen

J. Peng · Y. Wang · R. Wang (✉)
The Institute for Cognitive Neurodynamics, East China University of Science and Technology, No.130 Meilong Road, Shanghai 200237, China
e-mail: rbwang@163.com

R. Wang · W. Kong · J. Zhang
Key Laboratory of Brain Machine Collaborative Intelligence of Zhejiang Province, Hangzhou Dianzi University, Hangzhou, China

1 Introduction

The study on coding and decoding of neural signals is the essential and challenging part of neuroscience [1–3]; however, several issues are yet to be elucidated [4, 5]. At present, traditional coding theories, such as frequency coding, phase coding and time coding, have achieved a lot of research results. However, these theories or hypotheses still have certain limitations, and cannot explain how the brain encodes and decodes from a global perspective. In the past decade, studies from neuroscientists have relatively clarified the following aspects: the specific spike patterns of neurons in the visual cortex toward the physical characteristics of object location, shape, and prove that local field potential (LFP) contains useful information for decoding visual attention [6–8]. These results illustrate some of the characteristics of local coding in the brain, but the cerebral nervous structure is complex and multilevel; thus, an effective theory of neural coding should be inferred from the overall concept of the cerebral nerve activity. However, a mature theory on neural coding of the large-scale neuronal population is yet lacking, which is universally acceptable [9]. Also, a general coding theory to recognize and decipher cerebral nerve activity is not yet proposed. In the field of global coding research of the nervous system, the electrical activity of neurons needs to consume a lot of nerve energy in the brain, and the way of operation of the brain must obey two basic principles [10]: (1) Economy: the neuronal activity under supraliminal and subliminal stimulation was subjected to the energy minimization principle; (2) High efficiency: the signal transmission efficiency in the neural network was subjected to the principle of maximum energy utilization. Under the constraints of these two basic principles, how does neuroenergetics regulate the brain's operation and information coding? Based on the data from neuro-electrophysiological experiments, Wang–Zhang et al. initially proposed a novel biophysical model for studying the electrical properties of the coupled neurons [11], thereby proposing the theory and method of energy coding [12–16].

A critical feature of Wang–Zhang model lies in the function acquisition of neuronal membrane potential, which further revealed a unique corresponding relationship with the energy function [11]; this discovery was well confirmed by the Hodgkin–Huxley model [13]. The neuron encodes neural information via various spike patterns of membrane potentials, while the action potential and energy functions show a close correlation that render encoding the neural information possible by adopting the evolutionary pattern of energy. Our previous studies have demonstrated that the energetics method could be used to encode information invoked by different stimulations, including single neuronal spike and neural oscillations of different frequencies at the level of the neural network [12, 14, 16]. Since energy is a scalar unit, the energy consumed by individual neurons of a population can be superimposed on each other [15]. This calculation method could be adopted to avoid the difficulty of high-dimensional nonlinear coupling enclosed in the other coding theory. On the basis of the single neuronal energy function, we also probed the evolution of energy consumption of neuronal populations in the network model. When the network generated one pattern of energy distribution for one stimulation, we defined that this specific energy distribution encodes this one stimulation [12, 14, 16].

Presently, experimental studies on energy consumption in the nervous system mainly focus on the evaluation of experimentally observed and documented data. Current experimental neuroscience can quantitatively evaluate the changes in cerebral blood flow (CBF)-supplied energy demands according to blood oxygen level-dependent (BOLD) contrast signals, which is recorded with functional magnetic resonance imaging (fMRI) [17–22]. The identification of the concealed rule, which governs neural activity, from the experimental data is the key for research and development of a robot with human-like brains or intelligent computer. Differences in the CBF rise and the oxygen consumption ratio induce changes in the magnetic flux; as a result, fMRI can detect dynamic changes in the local blood flow in the corresponding brain regions within seconds of stimulation, i.e., termed as hemodynamics [23]. Generally, a significant CBF increase in the nervous system occurs in about 6–8 s post-stimulation on cortical neurons. Based on the relevant literature, an effective theory in current neuroscience to scientifically and rationally explain the phenomenon from the perspective of neural mechanisms is not yet available [24]. In addition, relevant studies on computer simulation of the experimental discovery and hemodynamics by neural modeling and calculation are lacking.

Glycogen is the primary energy storage in the human body, which is a large molecule polysaccharide composed of multiple glucose molecules. It is the energy reserve that the body can use rapidly. Glycogen in the human body is primarily reserved in the muscle and liver, accounting for 1–2% of the mass and weighing about 400 g in the muscle, while 6–8% of the mass and about 100 g in the liver. Additionally, less glycogen is reserved in the brain, accounting for 0.1% of the total brain weight and about 0.5–1.5 g [25], which is mainly stored in astrocytes. Pellerin and Magistretti proposed astrocyte-neuron lactate shuttle hypothesis (ANLSH) [26], which reflected the critical role of astrocytes in neural energy metabolism and hemodynamics. However, the function of brain glycogen remains to be fully elucidated. A large volume of studies [25, 27, 28] has revealed brain glycogen as a vital energy reserve and the material basis for brain activity—when the brain has increased activity, corresponding energy demands rise rapidly, whereas CBF is unable to alter timely, thereby resulting in blood glucose shortage. Consecutively, the glycolysis of brain glycogen rapidly occurs to fulfill the energy demands for the brain activity.

In addition to the critical role of NADH/NAD^+ in cellular energy metabolism, the concentration ratio of NADH/NAD^+ serves as the cell sensor for the regulation of blood supply [29]. In the energy metabolism of cells, including two different decomposition processes of glucose and lactic acid, NADH and NAD^+, respectively, participate in different decomposition processes as reactants (or products) and products (or reactants), forming a dynamic cycle between NADH and NAD^+. In addition, the cell also involves an important process of converting NADH to NAD^+, which occurs only when the cell is activated, and is closely related to the regulation of subsequent blood flow [29]. On the other hand, in the active state, if the equilibrium state of the transition between NADH and NAD^+ changes, the ratio of the NADH and NAD^+ concentrations will change, and as the ratio increases, the blood flow rise will be adjusted accordingly.

In order to explore the CBF delay phenomenon as observed in fMRI, this paper attempts to propose a physiological mechanism to produce hemodynamic phenomena from the perspective of energy metabolism. The ratio of NADH/NAD^+ concentrations was considered as the variable for CBF regulation, and introduces the role of brain glycogen in energy metabolism and hemodynamics. Based on this physiological mechanism, this paper builds a large-scale visual nervous system network based on the Wang–Zhang neuron model, and energetics coding method was adopted to experimentally decipher the physiological mechanism under hemodynamics and the corresponding changes in neuroenergetics. It quantitatively reproduced the hemodynamics observed in fMRI: a substantial CBF rise was delayed about 6–8 s to neuronal activation. This study predicted the negative energy during neural activity as the nature of cerebral hemodynamics, which based on a novel mechanism under neuronal activity identified in our previous studies [11]. Therefore, the significance of this study lies in providing a novel vision for establishing a global neural model of brain function and global neural coding in the future. Combined with previous studies, the present study provided an insight into the future scaffold of studies on brain working [5, 11–16, 30, 31].

2 Biophysical model of a neuron

In order to grossly calculate the energy consumption of neuronal network, Wang–Zhang et al. [11, 13, 30] proposed a novel biophysical model, and the structure is illustrated in Fig. 1. The differential equation is described as follows:

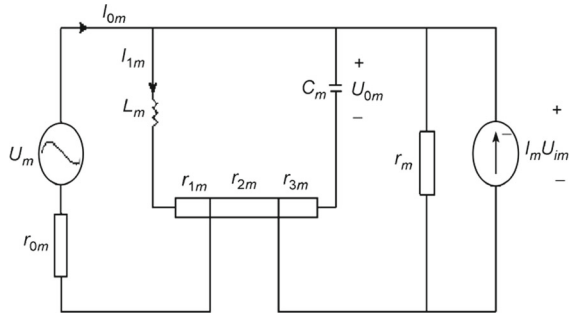

Fig. 1 Wang–Zhang biophysical model of a neuron [11]. C_m refers to the membrane capacitance, I_m refers to the total current input from external neurons, U_m was the voltage source, r_m refers to the resistance cross I_m, r_{0m} refers to the resistance cross U_m, and the membrane resistance was divided into three parts of r_{1m}, r_{2m} and r_{3m}. Moreover, the influx and outflux of a variety of charged ions through the ion channels generated a loop current, triggering the self-induction effect, which was equivalent to an inductor L_m

$$I_m = i_{1m} + \sum_{j=1}^{n} \left[i_{0m}(j-1) \sin(\omega_m(j-1)(t_j - t_{j-1})) \right] + i_{0m}(n) \sin(\omega_m(n)(t - t_n)) \tag{1}$$

$$\begin{cases} U_m = r_{0m} I_{0m} + r_{1m} I_{1m} + L_m \dot{I}_{1m} \\ I_{0m} = I_{1m} - I_m + \dfrac{U_{im}}{r_m} + C_m U_{0m} \\ U_{im} = C_m r_{3m} \dot{U}_{0m} + U_{0m} \end{cases} \tag{2}$$

$$L_m \dot{I}_{1m} + r_{1m} I_m = K_{1m} \dot{U}_{0m} + K_{2m} U_{0m} - r_{2m} I_m \tag{3}$$

wherein, $K_{1m} = C_m \left(r_{2m} + r_{3m} + \frac{r_{2m} r_{3m}}{r_m} \right)$, $k_{2m} = 1 + \frac{r_{2m}}{r_m}$

$$P_m = d_{1m} \dot{U}_{0m}^2 + d_{2m} \dot{U}_{0m} + d_{3m} \dot{U}_{0m} U_{0m} + d_{4m} U_{0m}^2 + d_{5m} U_{0m} + d_{6m} \tag{4}$$

As demonstrated in Fig. 2a, the neuronal action potentials obtained by simulation with Wang–Zhang neuron model were in agreement with the experimental data [11, 13]. However, the energetic changes in the action potential (Fig. 2b) in the present study were inconsistent with the conventional theory of neuroenergetics. During the process of action potential formation, the changes in the neuroenergetics were composed of two parts: oxygenated hemoglobin from blood, presenting as negative energy, which serves as an energy reserve, and the deoxygenated hemoglobin, presenting as positive energy, which serves as energy consumption [11–16].

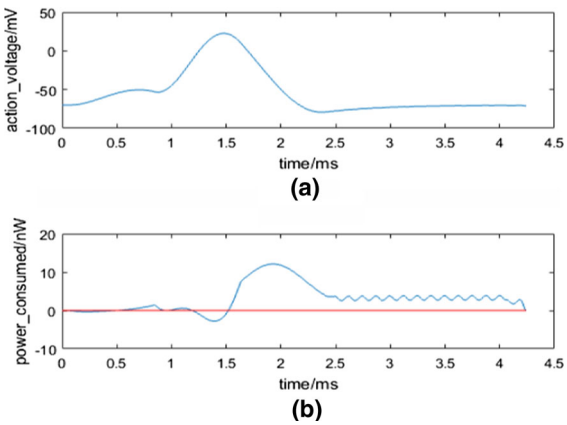

Fig. 2 Action potential and the corresponding energy function. **a** Shows the simulated neuron action potential; **b** shows the neuron power consumption curve. (Color figure online)

This novel energy calculation shows the neuron is an energy consumption as well as an energy reserve element. Zheng et al. and Parhizi et al. [28, 29] postulated a qualitative explanation for neurons and relevant gliocytes on the modulation of ion channel switch/glutamic acid cycle/glucose during action potential formation. The studies stated that the negative energy emerging in action potential was a process of energy reserve. Also, glucose and oxygen uptake from blood is greater than the consumption demands. Intriguingly, the stimulation of neurons triggers an increase in CBF, while depolarization demands oxygen consumption (without oxygen consumption yet at this point), mainly manifesting as energy uptake. During neuron repolarization, the energy reserve is exhausted, while the neuronal oxygen consumption ascends substantially, manifesting as energy consumption. Based on the action potential, neuron firstly absorbed the energy from CBF, followed by energy consumption, that goes round and round to reach a dynamic homeostasis. This indicates that the capability of the energy reserve is limited to a single neuron. The supply of glucose and oxygen in the bloodstream is usually sufficient, while if the neuronal energy reserve does not reach the upper limit, the neuron reserves energy. During the production of action potentials, the negative energy (reserved energy) will not be consumed, and the consumed energy is completely provided by the blood glucose while the negative energy is preserved by neuron for subsequent neural activity. This phenomenon indicates that the energy reserve of a single neuron should be an integer as a multiple of the counterpart in one action potential. Herein, e_0 represents the energy reserve of a single neuron in one action potential, e_a represents the average energy reserve of one neuron, e_i refers to the energy reserve of the i^{th} neuron, and E_0 refers to the energy reserve of the neural network. Therefore, the equations were as follows:

$$e_a = k_1 * e_0 \tag{5}$$

$$E_0 = \sum e_i \tag{6}$$

wherein, k_1 refers to adjustable parameters, and e_i fitted the Gaussian distribution if e_a was the mean, i.e., $e_i \sim N(e_a, u^2)$.

3 Gate control mechanism in hemodynamics

During neuronal excitation, the cyclic process between NADH and NAD^+ is involved in the decomposition of glucose and lactic acid. In cells, the breakdown of glucose begins with the glycolytic process of glucose. This process occurs in the cytoplasm, where glucose is broken down into pyruvate and produces a small amount of ATP under the action of enzymes, which is accompanied by the conversion of NAD^+ to NADH. The decomposition of lactic acid in cells involves both the process of decomposition into pyruvate under the action of enzymes, with the conversion of NAD^+ to NADH, and the process of reduction of pyruvate to lactic acid under the action of enzymes, which is an important way to convert NADH to NAD^+, and the transformation speed is very fast, while the specific direction of lactic acid decomposition depends on the relative concentrations of lactic acid and pyruvate in the cytoplasm. Eventually, the pyruvate in the cells participates in the tricarboxylic acid cycle (TCA), which is completely oxidized and decomposed in the mitochondria, producing CO_2 and H_2O and producing a large amount of ATP. In this process, NADH is first lost in the cytoplasm to generate NAD^+, which is the basic pathway for NADH to be converted into NAD^+. Then, NAD + is converted into NADH again in the mitochondria by enzymes.

From the perspective of energy metabolism, this paper attempts to use the concentration ratio of NADH/NAD^+ ($r = c_{(\mathrm{NADH})}/c_{(\mathrm{NAD^+})}$) as the cell sensor for the regulation of blood supply. Herein, v refers to changes in r, as shown in Eq. (7):

$$v(t) = \mathrm{sgn}(r_t - r_0) \tag{7}$$

wherein, r_t represents a concentration ratio of NADH versus NAD^+ at certain time points (t), while r_0 refers to the concentration ratio under a resting state.

On the other hand, NADH/NAD^+ cycle includes a transition of NADH into NAD^+ uniquely taking place as a consequence of cell activation, and this process is closely related to energy metabolism and the regulation of blood supply [26]. Herein, we considered this process as the release of reserved cellular energy and introduce the role of brain glycogen in energy metabolism and hemodynamics, underlying the mechanism of CBF regulation.

The changes in neural activity occur in ms after stimulation, owing to which, the brain is rapidly activated and accompanied by a rise in energy demands. However, CBF has not yet been altered. Therefore, the excessive energy demands trigger the release of reserved energy from neurons and glycolysis of glycogen in astrocytes. Thus, the excess energy demands are fulfilled by the energy reserve in neurons and glycogen in astrocytes (Fig. 3).

In Fig. 3, the energy demands rose in the brain upon stimulation, which triggered the release of reserved energy, thereby activating the transition of NADH into NAD^+, a process uniquely occurring as a result of cell activation. On the other hand, a rise in energy demands enhanced the lactate uptake from blood, thereby accelerating the transition of NAD^+ into NADH. Consequently, dynamic homeostasis of NADH and NAD^+ concentrations was formed that enabled a stable concentration ratio ($r = c_{(\mathrm{NADH})}/c_{(\mathrm{NAD^+})}$), and CBF remained unchanged. Moreover, a reduction in blood lactate contents accelerated the glycolysis of glycogen in astrocytes, which resulted in declining glycogen contents.

When the reserved energy was exhausted, the transition of NADH into NAD^+ would descend and simultaneously the lactate uptake from blood accelerated. Thus, the transition of NAD^+ into NADH was enhanced, which resulted in a rapid rise of cellular NADH contents and reduction of NAD^+ contents. Thus, the r value increased rapidly, thereby regulating the CBF rise (Fig. 4).

As shown in Fig. 4, after the reserved energy is completely exhausted, the additional energy demands of the brain were fulfilled by lactate breakdown, which was taken from blood by the cells, and it further

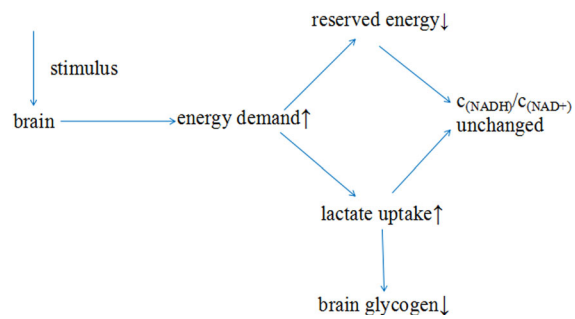

Fig. 3 Physiological mechanism underlying the lack of CBF alteration along with changing brain activity upon stimulation (own study). (Color figure online)

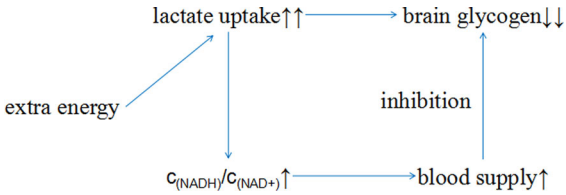

Fig. 4 Physiological mechanism underlying the increase in CBF (own study). (Color figure online)

accelerated the lactate uptake. This process led to a reduction in the content of blood lactate, thereby prompting the breakdown of brain glycogen; on the other hand, it resulted in an increased *r* value, thereby regulating a CBF increase. Subsequently, the CBF rise led to increased glucose uptake by astrocytes. This process inhibited glycolysis of glycogen, which halted the reduction of glycogen contents. When new dynamic homeostasis of NADH/NAD^+ concentrations was achieved in the cell, the substantially increased CBF was stabilized, and glycolysis, synthesis of astrocyte glycogen was balanced, that enabled stable glycogen contents.

4 Visual neural network and computing model

The visual system holds a distinct hierarchical structure as well as parallel and independent information processing pathways in response to different visual information [32, 33]. Given these two characteristics, the present study established a multilevel and multibranch network (Fig. 5), starting from the photoreceptor in the retina and ending at the V2 region of the visual cortex. The network encompassed six levels: the first level was comprised of cells in the retina (except for ganglion cells), the second level constituted the retinal ganglion cells, LGN was the third level, the fourth level consisted of the $4C_\alpha$ layer and $4C_\beta$ layer in V1 regions, the fifth level comprised of the III and IVB layers of V1 region, and the sixth level encompassed the V2 region (The 4 layer of V1 region can be further divided into three sublayers of 4A/4B/4C, and 4C can be divided into further two sublayers of $4C_\alpha$ and $4C_\beta$. The neurons in $4C_\alpha$ project to 4B layer, while neurons in the $4C_\beta$ project to layer 3. Therefore, the fifth level was constituted by layer 3 and 4B in V1 region). Considering the characteristics of visual neural network transmission and the neuroelectrophysiological phenomenon in experiments, the network input was designed as follows: an external stimulus was firstly imposed on a few photoreceptor cells in the first level that evoked activity of the other neurons within the same level via the inter-neuron coupling effect. Simultaneously, some neurons in the first level transmitted the neural activity to the second level via coupling with some neurons, and the signal reached the second level, which was gradually activated due to the intra-level coupling effect. Similarly, the signal was transmitted until the activation of large-scale neural network occurred at the last level (this study hypothesized that the inter-level transmission was unidirectional).

The number of individual types of cells in the pathway of rhesus macaques retina/LGN/cortex cited the data from their neurophysiological experiments [34]. Based on this statistic, in order to simplify the calculation without impacting the calculation effect, this study adopted the similarity principle on scaling-down of the statistical data. Furthermore, the ratio of various cells was close to the following: photoreceptor cell:ganglion cell:LGN cell:cell in the 4 layer of V1 region:cell in the 3 layer of V1 region:cell in V2 region = 100:1:2:50:20:120.

Table 1 shows the appropriate selection of multiple parameters. *N(i)* refers to the number of neurons in the functional cell population *i*, and *Nc(k)* refers to the number of neurons in the *k* level of the network, where the inter-neuron coupling probability in each functional cell population was reflected by *P(k)*. *M(i)* refers to the number of neurons in the functional cell population *i*, which were also influenced by the previous level of the network (functional cell population 1 and 2 at the first level referred to those receiving external stimulation). Thus, only *M(i)* neurons in the functional cell population *i* had a synaptic contact with the neurons in the previous level.

In the process of neural information transmission, coupled neurons in the network transmit signals by chemical synaptic contact, with synaptic delays of about 0.5–2 ms. In this study, τ_{mj} refers to the transmission time-lag when presynaptic neuron *j* transmitted the signal to the postsynaptic neuron *m*. This study presumed that all neurons in the network were excitatory neurons, and inter-neuron synaptic coupling strength was conventionally a random value within the range of uniform statistical distribution

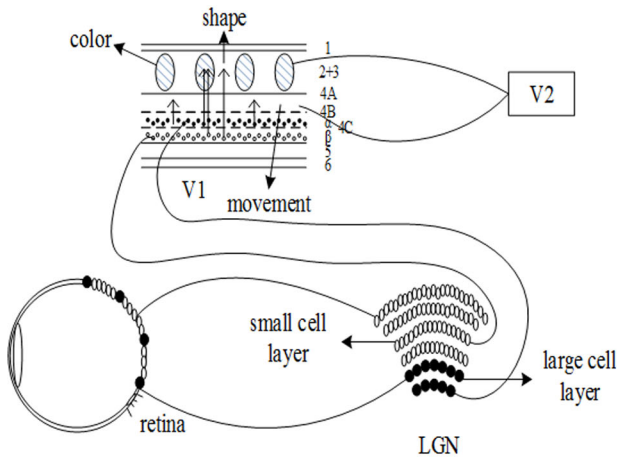

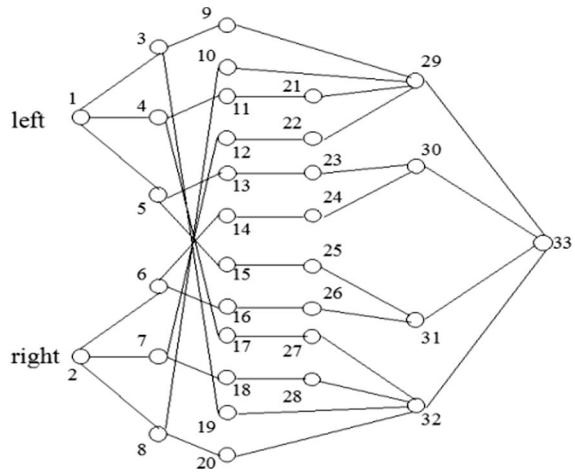

Fig. 5 The anatomical structure of the visual system and the hierarchical structure of the corresponding visual neural network. In the network, the hollow circle refers to the functional cell population constituted by relevant cells (namely a functional regional network); the straight line represents the synaptic contact between two functional cell populations; the number represents the label given according to the functional cell population: 1/2 (photoreceptor, bipolar cell), 3/8 (non-P/non-M type nerve cell), 4/7 (P type ganglion cell), 5/6 (M type ganglion cell), 9/10/19/20 (granular cell in LGN), 11/12/17/18 (small cell in LGN), 13/14/15/16 (large cell in LGN), 21/22/27/28 (cell in the 4Cβ layer of V1 region), 23/24/25/26 (cell in the 4Cα layer of V1 region), 29/32 (cell in the 3 layer of V1 region), 30/31 (cell in the 4B layer of V1 region), and 33 (cell in V2 region)

Table 1 Parameter selection for the visual neural network

Functional cell population	1	2	3	4	5	6	7	8	9	10	11	12	13	14	15	16	17	18	19	20
$N(i)$	1500	1500	5	5	5	5	5	5	5	5	5	5	5	5	5	5	5	5	5	5
$M(i)$	300		5																	
Layer k	1		2						3											
$P(k)$	0.3		1						1											
Nc(k)	3000		30						60											

Functional cell population	21	22	23	24	25	26	27	28	29	30	31	32	33
$N(i)$	100	100	100	100	100	100	100	100	300	300	300	300	3600
$M(i)$	20								60				800
Layer k	4								5				6
$P(k)$	0.8								0.5				0.3
Nc(k)	800								1200				3600

[35]. In order to stably probe the spike feature of the large-scale neuronal network, we postulated the coupling strength of two randomly coupled neurons as a fixed value (0.06) in the subsequent calculations. Moreover, according to the Hebbian principle of plasticity [36], each time when the presynaptic neuron j spikes an action potential, its coupling effect with the linked postsynaptic neuron would be enhanced during the neural pulse transmission. In addition, the present study simplified the plasticity of synapse and postulated that the increasing value of each coupling strength was L-fold of the initial value, which was reflected by the equation: $\omega = \omega * (1 + L)$. In the simulation, it was designated as $L = 0.02$.

Nonetheless, the plasticity of synaptic coupling strength has an appropriate threshold [37] that does not alter while ascending to a specific degree; in this study, value 1.5 was designated as the upper limit of the coupling strength.

The operation mode of this network was as described below:

1. Stimulation received by neuron i at time t was:

$$S_m(t) = \sum \omega_{mj} \times Q(t - \tau_{mj}, j) \tag{8}$$

2. Current received by neuron i at time t was:

$$I_m(t) = \begin{cases} i_{m1} + \sum_{j=1}^{n} [i_{0m}(j-1)\sin(\omega_m(j-1)(t_j - t_{j-1}))] + i_{0m}(n)\sin(\omega_m(n)(t - t_n)) \\ \text{if} \quad S_m(t) > \text{th} \\ i_{m1} \quad \text{if} \quad S_m(t) < \text{th} \end{cases} \tag{9}$$

3. $I_m(t)$ was substituted into Eq. (3) to obtain the solution of membrane potential $U_{0m}(t)$
4. The calculated value of Eq. (3) $U_{0m}(t)$ was substituted into Eq. (4) for power calculation to obtain the solution of neuronal power consumption $P_m(t)$
5. The total energy consumed by the neural network $P(t)$ was:

$$P(t) = \sum P_m(t) \tag{10}$$

6. According to the above proposed physiological mechanism, the energy source consumed by the neural network included three parts: the main part was derived from blood glucose breakdown, marked as $P_{g1}(t)$, while the remaining parts were obtained from the energy reserve and glycolysis of brain glycogen, marked, respectively, as $P_s(t)$ and $P_{g2}(t)$. The equation was as follows:

$$P(t) = P_{g1}(t) + P_{g2}(t) + P_s(t) \tag{11}$$

Among these:

$$\begin{cases} P_{g1}(t) = a * |P(t)| + v(t) * f(t) * |P(t)| \\ P_s(t) + P_{g2}(t) = b * P(t) - v(t) * f(t) * |P(t)| \\ P_s(t) = c * \text{sgn}(E(t)) * P(t) \end{cases}$$

In the above equations, $S_m(t)$ represents the sum of stimulation neuron m received at the time t; $Q(t, j)$ indicates the action potential release state of the jth neuron at time t, the neuron resting value is 0, and the action potential is 1 when the action potential is issued. In the simulations, since the neurons of the first level only generated grading changes in the membrane potentials, the Q value of the first-level neurons is taken as: $Q = S(t)$. $f(t)$ represents the blood flow rise function. This paper uses a one-dimensional quadratic function to simulate, which is taken as:

$$f(t) = \frac{-[t - (t_m - t_0)]^2}{k_2 * t_m^2} + \frac{1}{k_2} \tag{12}$$

wherein, t_0 represents the time when the stored energy is exhausted, and other parameters were taken as values according to the relevant experiment results [38]: a = *20/23*, b = 3/23, c = 7/115, k_2= 3, t_m= 1000 ms.

5 Results and analysis of model computing

Relevant network parameters are listed in Table 1. Moreover, individual neurons in the network were assigned sequence numbers: 1–1500 responded to neurons in the first functional cell population; 1501–3000 responded to neurons in the second functional cell population; the last 3600 numbers responded to neurons in the 33rd functional cell population of the last level. The total number of neurons in the network is N = 8690, which were sequentially numbered from 1 to 8690. Based on the above mathematical models, the simulation was conducted using MATLAB software. Continuous application of current stimulation imposed on a small portion of neurons in the network, including 1–300 neurons in the first functional cell population and 1501–1800 neurons in the second functional cell population of the first level, the stimulation intensity is $I(t) = 70.7\,\mu\text{A}$. Figure 6 displays the overall network neural activity and changes in the blood glucose energy supply.

Figure 6a demonstrates a rapid transmission of information in the neural network. At the time point of about 1200 ms, the overall neural activity reached a peak and stabilized gradually that indicated the state of synchronous oscillation was achieved rapidly by the overall network. While comparing Fig. 6a with b, the starting phase of stimulation revealed that the energy supply of blood glucose rose along with increased neural activity in the network; when the neural activity

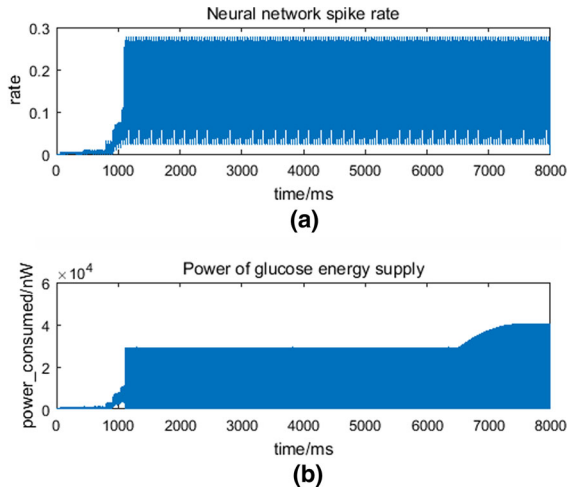

Fig. 6 Neural activity of the visual neural network and energy supply of blood glucose at the corresponding time points. The horizontal ordinate represents time points, and persistent strong stimulation was imposed on a portion of network neurons starting from the time point of 10 ms. **a** The vertical ordinate represents the overall network spike rate $R(t) = n(t)/N$, in which, $n(t)$ refers to the total number of neurons across the entire network, generating pulse spike at the time point t. **b** The vertical ordinate represents the power of energy supply by blood glucose during the entire process of network operation. (Color figure online)

peaked and gradually moved to stabilization, the same trend was shown in energy supply of blood glucose. However, until by about 6500 ms, this stabilization was interrupted, and the neural network activity was still stabilized, whereas the energy supply of blood glucose increased substantially rising, which was stabilized by 7500 ms. Figure 7 displays the magnified illustration of this process.

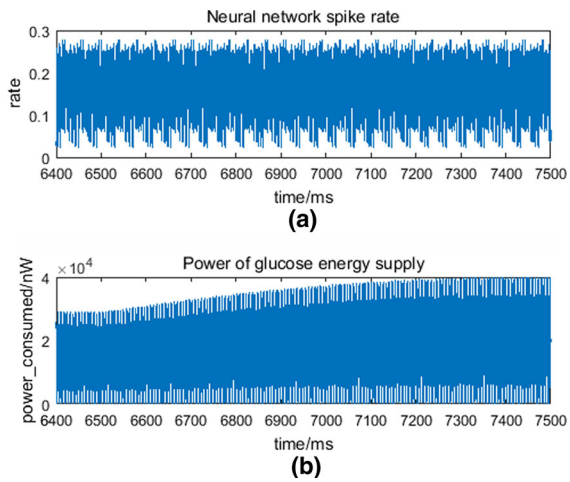

Fig. 7 Magnified diagram of 6400 $\sim$ 7500 ms. **a** Shows the neural activity of the visual neural network; **b** shows the energy supply of glucose in the blood. (Color figure online)

The simulation results show that the neural activity of the whole network peaks at around 1200 ms, while the blood glucose supply peaks at around 7500 ms, with a delay of about 6300 ms. On the other hand, the energy supply of glucose in the blood can indirectly reflect the change of blood flow, where the glucose supply increases greatly at around 6500 ms, which can directly reflect the large increase of blood flow. Therefore, the simulation results reproduce the hemodynamic phenomenon in fMRI experiments: after 6–8 s of activation of the brain region, cerebral blood flow will increase significantly.

Figure 8 displays the changes in the network neural activity and energy consumption during the above process. The figure showed that before 1200 ms, the starting phase of stimulation, network energy consumption rose along with increasing neural activity, while after 1200 ms, when the neural activity peaked and stabilized gradually, the corresponding energy consumption as well reached a peak and gradually moved to stabilization. This phenomenon indicated that the network energy consumption corresponded to the neural activity. The combination of Figs. 6 and 8 showed that after 1200 ms, the neural network activity, and corresponding energy consumption were constantly in the stable state, thereby indicating the

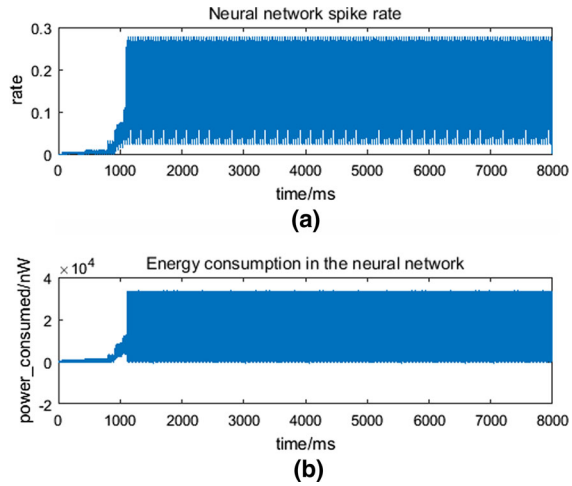

Fig. 8 Neural activity and energy consumption in the network. **a** Recorded the changes in overall network spike rate, while **b** reflected the energy consumption at the corresponding time points. (Color figure online)

substantial rise of blood glucose energy supply at about 6500 ms was no result of elevated energy consumption by the neural network. This implied that the delay in the increase of blood glucose energy supply was caused due to other reasons.

To explore the relationship between energy consumption and blood glucose supply in the network, we also recorded the energy consumption of the network and the change in blood glucose supply over time (see Fig. 9). The figure showed the blood sugar supply initially increases with the increase of energy consumption of the network. At about 1200 ms, the energy consumption of the network reaches a peak and tends to be stable, and the blood sugar supply tends to be stable. However, the energy consumption of the network is significantly higher than that of the blood glucose, indicating that the energy supply of glucose in the blood cannot fully satisfy the energy demand of the neural network. When this state continues until at about 6500 ms, the energy consumption of the network is still stable, but the blood glucose supply begins to increase substantially until peaks and stabilizes again at about 7500 ms. At this time, the blood glucose supply is significantly higher than the energy of the network consumption.

According to the physiological mechanism proposed, the capacity of glucose energy supply was limited under the normal blood flow, and when the entire neural network was activated, the energy consumption was maximal and the energy supply by glucose was maximal with respect to the normal blood flow; however, it still could not fulfill the energy demands of the entire neural network, which is consistent with the results of Fig. 9. On the other hand, $r = c_{(\mathrm{NADH})}/c_{(\mathrm{NAD^+})}$ acted as a cell-based biosensor in the CBF regulation, and when the network energy reserve was completely exhausted, the r-value would rapidly rise to a raised CBF increase, thereby elevating the capacity of blood glucose energy supply. In this regards, we focused on the changes in the energy reserve of the neural network and the energy supply of blood glucose during the entire process. Figure 10 documents the altered network energy reserve and energy supply of blood glucose over a period during the entire process. Figure 10a records the changes in energy reserve of the entire network, while Fig. 10b records the corresponding changes in the energy supply of blood glucose. The figure displayed that before 1200 ms, no obvious changes occurred in the network energy reserve, while energy supply of the blood glucose gradually rose; after 1200 ms, the network energy reserve underwent a significant decline, while the energy supply of blood glucose peaked and stabilized gradually. Furthermore, by about 6500 ms, the network energy reserve was completely exhausted, and the corresponding energy supply of blood glucose started a substantial rise (Fig. 11).

The above simulation results revealed that at about 1200 ms, the neural network was gradually activated,

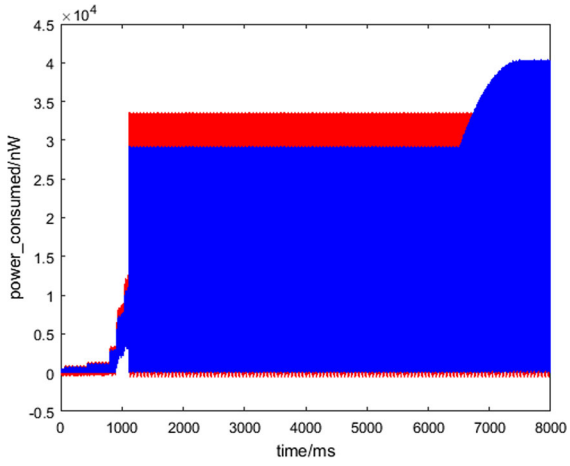

Fig. 9 The energy consumption of the network and the of blood glucose supply. Red indicates the energy consumption curve of the network; blue indicates the curve of blood glucose energy supply over time. (Color figure online)

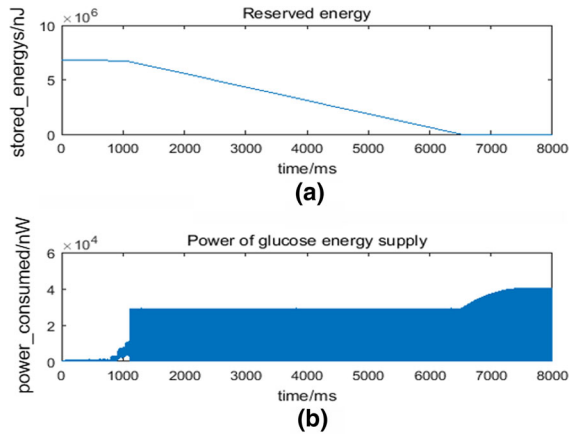

Fig. 10 Network energy reserve and changes in glucose energy supply. **a** Records the energy storage changes of the entire network, and **b** records the changes in the corresponding blood glucose supply. (Color figure online)

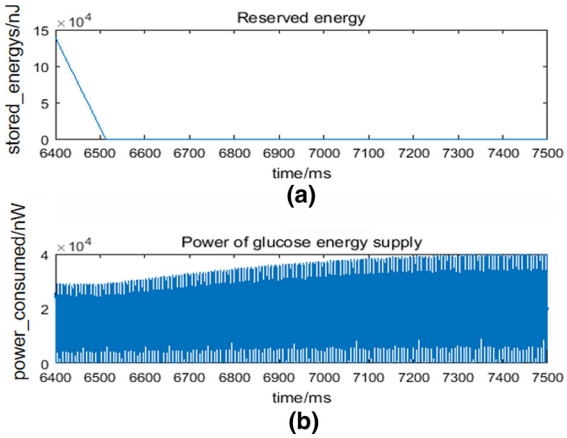

Fig. 11 Magnified illustration of 6400–7500 ms. (Color figure online)

and energy consumption in the neural network rose substantially, and although the energy supply of the blood glucose reached a maximum of normal blood flow, it could not meet the energy demands completely that led to the consumption of the energy reserve. At about 6500 ms, the energy reserve in the neural network was completely exhausted, causing the ratio r to increase rapidly, causing a large increase in blood flow, at which time the supply of glucose in the blood begins to increase substantially.

6 Summary

Hemodynamics intuitively reflected the relationship between activation of brain regions and CBF, as well as that between CBF and energy metabolism. This study proposed a physiological mechanism for generating hemodynamic phenomena from the perspective of energy metabolism, which predicts the nature of brain hemodynamics is the negative energy mechanism during neural activity. In a cell, $r = c_{(\mathrm{NADH})}/c_{(\mathrm{NAD^+})}$ acts as a cell-based biosensor in the CBF regulation that increases with increasing r. The greater the Δr, the greater the ΔCBF. Under normal condition, cellular NADH and NAD^+ are in the state of mutual transition, reaching a dynamic homeostasis, that does not enable any obvious changes in the ratio r. When the brain receives external stimulation or brain activity increases suddenly, the energy consumption rises rapidly, causing shortage blood glucose. Thus, cellular energy reserve and brain glycogen are rapidly consumed as the emergency energy. In this process, the consumption of energy reserve prompts the transition of NADH into NAD^+, while the glycolysis of brain glycogen suppresses the transition of NADH into NAD^+ but promotes the transition of NAD^+ into NADH, that enables no obvious changes in the ratio r, thereby avoiding significant changes in CBF. By the time, the energy reserve of the neural network is completely exhausted, the transition of NADH into NAD^+ loses one pathway, and the glycolysis of brain glycogen is accelerated. This further suppresses the transition of NADH into NAD^+ while promoting the transition of NAD^+ into NADH, consequently increasing r and causing a substantial increase in CBF. Conversely, increased CBF suppresses the glycolysis of brain glycogen, and CBF is elevated considerably to peak prior to stabilization until new dynamic homeostasis of NADH/NAD^+ mutual transition is reached. At this point, the energy consumption of the neural network can be provided sufficiently by blood glucose and oxygen.

Based on the above theories and physiological mechanisms, the present study built a large-scale visual neural network according to the anatomical structure of the visual system by using Wang–Zhang neuron model. A computer simulation was adopted to calculate the changes in neural activity of network neurons and network energy consumption within 8000 ms. The results showed that within 1200 ms after stimulation, the neural activity of network neurons and energy consumption presented stepwise changes over time, which was in agreement with the level-to-level transmission of network information. Subsequently, the energy reserve of the neural network started to decline obviously, and by 6500 ms, the energy reserve was exhausted completely, while the energy supply of blood glucose increased substantially prior to stabilization. Taken together, the energy supply of blood glucose could indirectly reflect the CBF changes and a substantial rise in energy supply of blood glucose at about 6500 ms reflected a substantial CBF rise. Until 7500 ms, the glucose supply peaked, which was delayed by about 6300 ms compared to the time when the neural activity of the neural network peaked, thereby reproducing the hemodynamics observed with fMRI: the level of CBF would not rise substantially until 6–8 s after activation of brain regions [23].

This study proposed a physiological mechanism for generating hemodynamic phenomena from the perspective of energy metabolism, which predicts the nature of brain hemodynamics is the negative energy mechanism during neural activity. It would provide a scientific basis for establishing the nerve model of the overall brain function and neural coding. Thereby, this study can reveal the overall nature of functional brain activity that would provide a novel viewpoint and method for theoretical study, modeling, and computing [39–42].

Acknowledgements This work was supported by the National Natural Science Foundation of China (NSFC) (11872180, 12072113, 61633010, 61473110)

Compliance with ethical standards

Conflict of interest The authors declare that they have no conflict of interest.

References

1. Jafakesh, S., Jahromy, F.Z., Daliri, M.R.: Decoding of object categories from brain signals using cross frequency coupling methods. Biomed. Signal Process. Control **27**, 60–67 (2016)
2. Zhu, F., Wang, R., Pan, X., Zhu, Z.: Energy expenditure computation of a single bursting neuron. Cogn. Neurodyn. **13**, 75–87 (2019)
3. Taghizadeh-Sarabi, M., Daliri, M.R., Niksirat, K.S.: Decoding objects of basic categories from electroencephalographic signals using wavelet transform and support vector machines. Brain Topogr. **28**, 33–46 (2015)
4. McLaughlin, D.W.: Ruling out and ruling in neural codes. Proc. Natl. Acad. Sci. PNAS. **106**(14), 5936–5941 (2009)
5. Parhizi, B., Daliri, M.R., Behroozi, M.: Decoding the different states of visual attention using functional and effective connectivity features in fMRI data. Cogn. Neurodyn. **12**, 157–170 (2018)
6. Wang, G., Wang, R.: Simulation of retinal ganglion cell response using fast independent component analysis. Cogn. Neurodyn. **12**(6), 615–624 (2018)
7. Teng, C., Cheng, Y., Wang, C., Ren, Y., Weiyong, X., Jin, X.: Aging-related changes of EEG synchronization during a visual working memory task. Cogn. Neurodyn. **12**, 561–568 (2018)
8. Zhang, T., Pan, X., Xuying, X., Wang, R.: A cortical model with multi-layers to study visual attentional modulation of neurons at the synaptic level. Cogn. Neurodyn. **13**, 579–599 (2019)
9. Braga, R.M., Sharp, D.J., Leeson, C., Wise, R.J.S., Leech, R.: Echoes of the brain within default mode, association, and heteromodal cortices. J. Neurosci. **33**, 14031–14039 (2013)
10. Laughlin, B.S., Sejnowski, T.J.: Communication in neuronal networks. Science **301**, 1870 (2003)
11. Wang, R., Tsuda, I., Zhang, Z.: A new work mechanism on neuronal activity. Int. J. Neural Syst. **25**(03), 1450037 (2015)
12. Wang, Z., Wang, R.: Energy distribution property and energy coding of a structural neural network. Front. Comput. Neurosci. **100**, 100 (2014). https://doi.org/10.3389/fncom.2014.00014
13. Wang, R., Wang, Z., Zhu, Z.: The essence of neuronal activity from the consistency of two different neuron models. Nonlinear Dyn. (2018). https://doi.org/10.1007/s11071-018-4103-7
14. Wang, Z., Wang, R., Fang, R.: Energy coding in neural network with inhibitory neurons. Cogn. Neurodyn. **9**(2), 129–144 (2015)
15. Wang, R., Zhang, Z., Chen, G.: Energy function and energy evolution on neural population. IEEE Trans. Neural Netw. **19**, 535–538 (2008)
16. Zhu, Z., Wang, R., Zhu, F.: The energy coding of a structural neural network based on the Hodgkin–Huxley model. Front. Neurosci. **12**, 122 (2018)
17. Hyder, F., Rothman, D.L., Shulman, R.G.: Total neuroenergetics support localized brain activity: implications for the interpretation of fMRI. Proc. Natl. Acad. Sci. (PNAS) **99**(16), 10771–10776 (2002)
18. Smith, A.J., Blumenfeld, H., Behar, K.L., Rothman, D.L., Shulman, R.G.: Cerebral energetics and spiking frequency: the neurophysiological basis of fMRI. Proc. Natl. Acad. Sci. (PNAS) **99**(16), 10765–10770 (2002)
19. Raichle, M.E., Gusnard, D.A.: Appraising the brain's energy budget. Proc. Natl. Acad. Sci. (PNAS) **99**(16), 10237–10239 (2002)
20. Laughlin, B.S.: Energy as a constraint on the coding and processing of sensory information. Curr. Opin. Neurobiol. **11**, 475–480 (2001)
21. Levy, W.B., Baxter, R.A.: Energy efficient neural codes. Neural Comput. **8**(3), 531–543 (2003)
22. Fox, M.D., Raichle, M.E.: Spontaneous fluctuations in brain activity observed with functional magnetic resonance imaging. Nature **8**, 700–711 (2007)
23. Buxton, R.B.: Modeling the hemodynamic response to brain activation. NeuroImage **23**, S220–S233 (2004)
24. Amaro Jr., E., Barker, G.J.: Study design in fMRI: basic principles. Brain Cogn. **60**, 220–232 (2006)

25. Brown, A.M.: Brain glycogen re-awakened. J. Neurochem. **89**, 537–552 (2004)
26. Pellerin, L., Magistretti, P.J.: Glutamate uptake into astrocytes stimulates aerobic glycolysis: a mechanism coupling neuronal activity to glucose utilization. Proc. Natl. Acad. Sci. U.S.A. **91**, 10625–10629 (1994)
27. Brown, A.M.: Energy transfer from astrocytes to axons: the role of CNS glycogen. Neurochem. Int. **45**, 529–536 (2004)
28. DiNuzzo, M., Mangia, S., Maraviglia, B., Giove, F.: The role of astrocytic glycogen in supporting the energetics of neuronal activity. Neurochem. Res. **37**, 2432–2438 (2012)
29. Mintun, M.A.: Increased lactate/pyruvate ratio augments blood flow in physiologically activated human brain. PNAS **2**, 659–664 (2004)
30. Wang, R., Zhu, Y.: Can the activities of the large scale cortical network be expressed by neural energy? A brief review. Cogn. Neurodyn. **1**, 1–5 (2016)
31. Yao, M., Wang, R.: Neurodynamic analysis of Merkel cell–neurite complex transduction mechanism during tactile sensing. Cogn. Neurodyn. **13**, 293–302 (2019)
32. Özgör, C., Özgör, S.Ş., Duru, A.D., Işoğlu-Alkaç, Ü.: How visual stimulus effects the time perception? The evidence from time perception of emotional videos. Cogn. Neurodyn. **12**, 357–363 (2018)
33. Shou, T.: The Brain Mechanism of Visual Information Processing. China Science and Technology University Press, Shatin (2010)
34. Barlow, H.B.: Critical limiting factors in the design of the eye and visual cortex. Proc. R. Soc. Lond. **212**, 1–34 (1981)
35. Rubinov, M., Sporns, O., Thivierge, J.-P., Breakspear, M.: Neurobiologically realistic determinants of self-organized criticality in networks of spiking neurons. PLoS Comput. Biol. **7**(6), e1002038 (2011)
36. Wennekers, T., Plam, G.: Syntactic sequencing in Hebbian cell assemblies. Cogn. Neurodyn. **3**, 429–441 (2009)
37. Le Van, Q.M., Martinerie, J., Navarro, V., Baulac And, M., Varela, F.J.: Characterizing neurodynamic changes before seizures. J. Clin. Neurophysiol. **3**, 191–208 (2001)
38. Lin, A.-L., Fox, P.T., Hardies, J., Duong, T.Q., Gao, J.-H.: Nonlinear coupling between cerebral blood flow, oxygen consumption, and ATP production in human visual cortex. Proc. Natl. Acad. Sci. PNAS. **18**, 8446–8451 (2010)
39. Wang, Y., Xuying, X., Wang, R.: Neural energy mechanism and neurodynamics of memory transformation. Nonlinear Dyn. **97**, 697–714 (2019)
40. Xu, X., Wang, Y., Wang, R.: Energy features in spontaneous up and down oscillations. Cogn. Neurodyn. (2020). https://doi.org/10.1007/s11571-020-09597-3
41. Wang, Y., Xuying, X., Wang, R.: The place cell activity is information-efficient constrained by energy. Neural Netw. **116**, 110–118 (2019)
42. Zhu, F., Wang, R., Aihara, K., et al.: Energy-efficient firing patterns with sparse bursts in the Chay neuron model. Nonlinear Dyn. **100**, 2657–2672 (2020)